Journal of the Serbian Chemical Society
JSCS-info@shd.org.rs • www.shd.org.rs/JSCS
J. Serb. Chem. Soc. *90* (7–8) 899–913 (2025)
JSCS–5428
Original scientific paper
Published 27 August, 2025

Molecular docking's pioneering role in materials science. Metal ion site-preference in fluorapatite

MARIJA M. PETKOVIĆ-BENAZZOUZ[1], IGOR RADOVIĆ[2], DUŠAN V. MILOJKOV[3] and GORAN V. JANJIĆ[4]*

[1]*University of Belgrade–Faculty of Physics, Studentski Trg 12, Belgrade, Serbia,* [2]*Department of Dental Pathology, Faculty of Medicine, University of East Sarajevo, Studentska 5, Foča, Bosnia and Hercegovina,* [3]*Institute for Technology of Nuclear and Other Mineral Raw Materials, Franše d' Eperea 86, Belgrade, Serbia and* [4]*University of Belgrade–Institute of Chemistry, Technology and Metallurgy, National Institute of the Republic of Serbia, Njegoševa 12, Belgrade, Serbia*

(Received 2 February, revised 11 March, accepted 11 April 2025)

Abstract: Originally created for biological systems, molecular docking has proven to be useful to predict metal ion binding locations and affinities in materials. By using this novel approach, it was possible to estimate the binding energies of Ca^{2+}, Sr^{2+}, Mn^{2+}, Cu^{2+} and Pr^{3+} for two different calcium sites in fluorapatite. The data obtained from the crystal structures of doped fluorapatites showed a good agreement with the docking research. The interpretation of docking results was made easier by combining results from DFT calculations with geometrical analysis of crystal structures of small molecules. Notably, this strategy is more favourable than previously used theoretical approaches due to the computational efficiency and the demonstrated reliability.

Keywords: electrostatic model; binding energy.

INTRODUCTION

Fluorapatite (FAp, $Ca_5(PO_4)_3F$) represents the prevailing form of calcium phosphate following hydroxyapatite (HAp) in biological matrices. Due to its presence in natural systems, synthetic fluorapatite is frequently employed as a biocompatible material for applications such as bone replacement and the coating of bone prostheses.[1] The integration of materials incorporating both HAp and FAp holds significant promise in advancing dental surgery and conservative dentistry.

Fluorapatite comprises three ions (F^-, Ca^{2+} and PO_4^{3-}), classified under the space group $P6_3/m$. The compositions of fluorapatite minerals found in nature differ from these ideal compositions because the crystal lattice of FAp is tolerant

* Corresponding author. E-mail: goran.janjic@ihtm.bg.ac.rs
https://doi.org/10.2298/JSC250202028B

of various isomorphic substitutions. Fluorapatite's structure and numerous ionic bonds make it an excellent host for various substitutes. Four distinct types of substitution can be defined based on earlier research.[2] The primary and universally acknowledged substitution within the context of fluorapatite is the F^- substitution. The singular substitution causing changes to the crystal structure involves Ca^{2+} substitution, which can manifest at two distinct sites, Ca(1) and Ca(2). In a general sense, the substitution process is contingent upon the relative size and charge of metal ion substituent. Specifically, for the Ca^{2+} sites, the substituent radius may vary within the range of 0.95 to 1.35 Å.[4] Small cations in the M^{2+} category occupy the Ca(1) site, as larger substituents exhibit a preference for the Ca(2) site.[3,4] Monovalent ions (K^+, Na^+) frequently engage in substitution at the Ca(1) site, resulting in the creation of vacancies within the F^- sites and occasionally within the Ca(1) site.[3] The greater affinity of Ag^+ for the Ca(1) site has been confirmed.[5] In cases where the substituent is divalent, such as Sr^{2+}, Pb^{2+} or Mg^{2+}, the Ca(2) the site is preferentially targeted for substitution.[6,7] Furthermore, the substitution by a trivalent substituent is strategically employed in the fabrication of fluorescent materials tailored for diverse applications.[6,8–10] Rare earth ions exhibit the capability to undergo substitutions in both cation positions.[9,11]

Various theoretical methodologies have been developed for the precise evaluation of material properties and the prediction of thermodynamic data. The present research is oriented towards exploring the potential application of molecular docking to predict the site-preferences of particular metal ions to fluorapatite, as well as towards the changes in stability of the crystal structure induced by the doping of these metal ions were quantified. As a validation of applicability, the theoretically predicted parameters were compared with the experimentally determined values.

METHODOLOGY

CSD analysis

From the Cambridge Structural Database (CSD),[12] all structures containing the M–O fragment were extracted (M = Ca^{2+}, Sr^{2+}, Mn^{2+}, Cu^{2+} or Pr^{3+}). For the purposes of understanding the binding geometry of the mentioned ions to fluorapatite, two geometrical parameters were analysed: the lengths of the M–O bonds and the number of bonded X atoms to the metal ion (or the number of M–X bonds). To achieve the most reliable analysis of geometric data, only structures from the CSD that fulfil the following criteria were analysed: error-free coordinates according to the criteria used in the CSD; not disordered structures; no powder structures; no polymer structures; determined 3D coordinates; the crystallographic R factor is less than 10 %.

Density functional theory (DFT) calculations

Given that the interactions between metal ions and phosphate groups exert the most significant influence on metal ion binding, the chosen model system for the assessment of interaction strength comprises solely these two molecular species. Calculations at the wb97xd/x2c-TZVPall level of theory, which proved to be the most relevant (described in more detail in

Supplementary material to this paper, SM1), were conducted to assess the interaction strength of the phosphate group with other metal ions.

Molecular docking study

The rigid structures of the receptors corresponding to calcium binding sites 1 and 2 (Ca(1) and Ca(2)) were extracted from the crystal structure of hexagonal ($P6_3/m$) fluorapatite with the formula $Ca_5(PO_4)_3F$ and refined to $R = 0.025$.[13] The preparation of targets and ligands (metal ions) for the docking study was conducted using the AutoDockTools program, and the docking calculations were executed with the AutoDock program.[14] A grid box of dimensions 12 Å×12 Å×12 Å, encompassing the entire target structure was employed to accommodate the investigated metal ions. Throughout the docking calculations, the structures of the targets were kept rigid, while the ligand (metal ion) had freedom of movement within the box. The Lamarckian genetic algorithm served as the search method, using 100 runs for each virtual screening. Analysis of the docking study results and visualization of outcomes, graphically representing the conclusions, were performed using the Discovery Studio software (BIOVIA Software product).[15] There are two commonly used sets of charges (Gasteiger and Kollman) in Autodock. In contrast to the classical docking calculation in the AutoDock program (Gasteiger or Kollman charges are used), this research employed an electrostatic model. Specifically, in the pdbqt files of targets, the calcium ions' charge was set to +2, and the fluoride ion's charge was set to –1. The total charge of the phosphate group is –3, and the partial charges of the oxygen atoms and phosphorus were determined through quantum-mechanical calculations. The phosphate group structure was optimized at the wb97xd/x2c-TZVPall level of theory, and the natural population analysis (NPA) charges were calculated. The calculated partial charges (+2.488 for P and –1.372 for O) were then entered into the pdbqt files of the targets. The charges of metal ions as ligands were set to +2 (for calcium, strontium, manganese and copper) or +3 (for praseodymium).

RESULTS AND DISCUSSION

CSD analysis

Molecular docking is a fast and useful computational technique widely used in drug discovery for identifying the binding affinity and the binding mechanism of small molecules (ligands) to biomolecules (receptors). While originally devised for applications in biological systems, this investigation departs from the customary usage of molecular docking methodologies by employing them to assess the binding affinities of specific metal ions (Ca^{2+}, Sr^{2+}, Mn^{2+}, Cu^{2+} and Pr^{3+}) for two distinct calcium binding sites within fluorapatite, which is a material of interest. In addition, the further goal of this research is to determine whether the molecular docking is a suitable tool for materials and an adequate technique to explain the experimental results, based on X-ray diffraction, for doped fluorapatite. In the context of this investigation, the structural attributes of sites 1 and 2 are delineated as comprising Ca(1) and Ca(2) coordination polyhedra (Fig. 1).

Calcium binding site 1 manifests as a nine-coordinated Ca(1) polyhedron, characterized by six abbreviated Ca–O bonds (shorter than 2.5 Å), defining an approximate trigonal prism, and three elongated Ca–O bonds (bond lengths of 2.764 Å) extending through the prism faces. From the supramolecular point of view, six phosphate groups are coordinated to the Ca(1) ion in site 1 (Fig. 1).

Among these, three phosphate groups exhibit bidentate coordination to Ca (Ca–O bond lengths of approximately 2.434 and 2.763 Å), while the remaining three groups demonstrate monodentate coordination (Ca–O bond lengths of 2.376 Å). The average length of Ca–O bonds at Ca(1) is around 2.524 Å. The Ca(2) polyhedron can be conceptualized as a CaO_5F octahedron, with Ca–O bond lengths of 2.348, 2.349, 2.375, 2.501 and 2.502 Å, and Ca–F bond of 2.310 Å. Nonetheless, the octahedral geometry experiences distortion owing to the presence of an additional (seventh) Ca–O bond (Fig. 1b), which is comparatively weaker than the aforementioned bonds, evidenced by a bond length of 2.700 Å. At Ca(2), five phosphate groups coordinate with the calcium ion, with only one group engaging in bidentate coordination (Ca–O bond lengths of 2.501 and 2.502 Å), while the remaining groups exhibit monodentate coordination. The average length of Ca–O bonds at site 2 is notably shorter at 2.441 Å compared to Ca(1) (2.524 Å), signifying heightened sensitivity to doped ion size in the binding of metal ions at Ca(2).

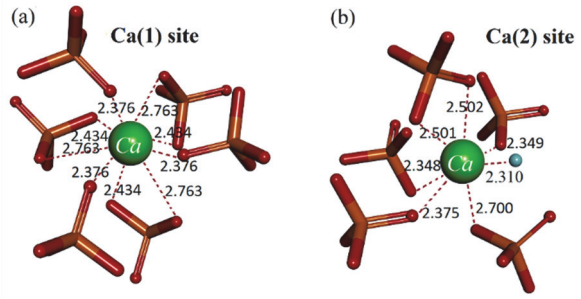

Fig. 1. Supramolecular profile of binding site 1 Ca(1) (a) and site 2 Ca(s) (b) in the crystal structure of fluorapatite.[13]

In order to determine whether the doping of fluorapatite with Sr^{2+}, Mn^{2+}, Cu^{2+} or Pr^{3+} lead to their coordination with phosphate groups, or the binding of metal ions has an electrostatically attractive character, the analysis of the crystal structures from the CSD was performed. The structures featuring M–O bonds (where M is Ca^{2+}, Sr^{2+}, Mn^{2+}, Cu^{2+} or Pr^{3+}) were extracted from the CSD, and the lengths of these M–O bonds, along with the metal ion environment, were systematically examined (Figs. 2 and S-1 of the Supplementary material). The environment was assessed by considering the number of M–X bonds (where X is any atom) achieved by the metal ion possessing at least one M–O bond. As previously explained, the binding of calcium ions to Ca(1) or Ca(2) site results in the formation of Ca–O and Ca–F bonds within the range of 2.3 to 2.8 Å (Fig. 1).

Taking this interval into consideration, it is deduced that all selected metal ions, with the exception of Mn^{2+}, can effectively substitute calcium ions in both sites. This substitution involves the establishment of covalent-coordination bonds with phosphate groups and fluoride ions in the respective sites (Fig. 2). Notably,

there is a lack of crystal structures in the CSD featuring Mn–O bonds longer than 2.6 Å, setting Mn^{2+} apart. This finding aligns with the analysis of the number of M–X bonds for individual metal ions (Fig. 2).

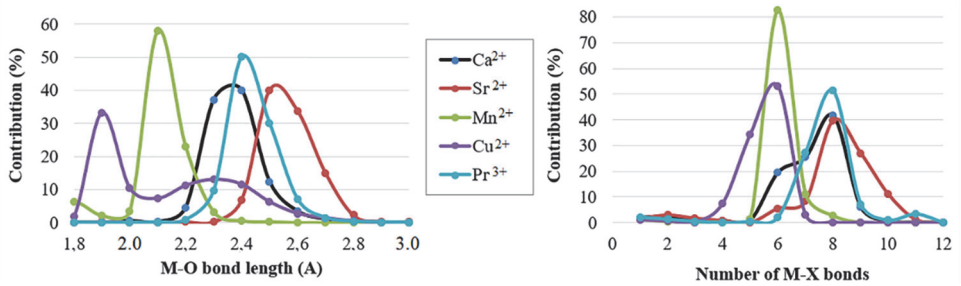

Fig. 2. Geometrical parameters for structures with M–O bonds (M: Ca^{2+}, Sr^{2+}, Mn^{2+}, Cu^{2+} or Pr^{3+}) extracted from crystal structures of small molecules, archived in the CSD.

Considering that Ca(1) site corresponds to a nine-coordinated polyhedron, while Ca(2) site corresponds to a seven-coordinated polyhedron, it is evident that all metal ions, excluding Mn^{2+}, can maintain the coordination geometry akin to the calcium ion following substitution. Specifically, there is an absence of crystal structures in the CSD depicting Mn^{2+} compounds concurrently featuring Mn–O bonds and Mn^{2+} with nine M–X bonds, a characteristic geometry associated with Ca(1) site.

DFT calculations

In a benchmark study, the model system comprised solely of Mn^{2+} and a phosphate group (Fig. S-2 of the Supplementary material) underwent examination using the wb97xd method with four distinct basis sets (def2-TZVP, jorge-TZP, x2c-TZVPall and dgauss-DZVP basis set). The investigation revealed that the x2c--TZVPall basis set exclusively produced a curve corresponding to the Lennard--Jones potential. This potential represents a mathematical framework elucidating interactions between two chemical entities at specific distances (Fig. S-2). Consequently, the x2c-TZVPall basis set was selected for assessing the strength of interactions between other metal ions (M^{n+}) and the phosphate group (Fig. 3).

Results derived from calculations at the wb97xd/x2c-TZVPall level of theory disclosed that the Ca^{2+} makes interactions with a strength ranging from –2550 to –2650 kJ mol^{-1}, within the distance range characteristic of Ca(1) and Ca(2) sites (2.3 to 2.8 Å). On the other hand, within the given distance range, the Sr^{2+} display slightly weaker interactions (from –2420 to –2550 kJ mol^{-1}). Interestingly, the Mn^{2+} exhibits interaction energies ranging from –3180 to –3390 kJ mol^{-1}, forming significantly stronger bonds with the phosphate ion. Cu^{2+} exhibits the strongest interactions of all the divalent ions, with interaction energies ranging from –3550 to –3770 kJ mol^{-1}. Pr^{3+} establishes the strongest interactions with phosphate group

(ranging from –4680 to –4940 kJ mol^{-1}), attributable to its elevated positive charge relative to other metal ions.

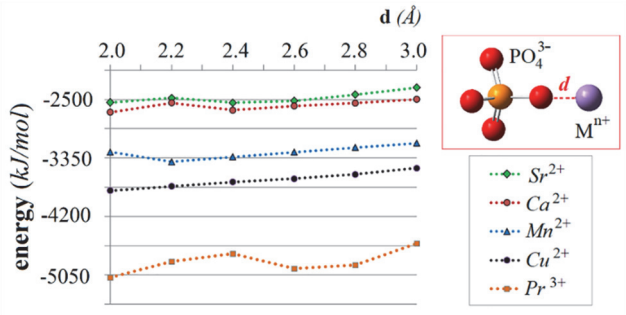

Fig. 3. Results of DFT calculations for evaluation of the interaction energies between the phosphate group and the metal M^{n+} (M^{n+}: Ca^{2+}, Sr^{2+}, Mn^{2+}, Cu^{2+} or Pr^{3+}). Parameter *d* represents the M···O distance, with the linear geometry of the interacting atoms and phosphorus atom (M···O–P angle is equal to 180°).

Molecular docking study

The molecular entities constituting Ca(1) and Ca(2) targets (Fig. 4), represent the phosphate groups and fluorides, with a cavity at the site of the central calcium ion. The incorporation of eight additional calcium ions on the surface of mentioned target structures (Fig. 4), resulted in the binding of metal ions only in the cavity. Calculated binding energies served as direct indicators of the investigated metal ions' affinities for specific sites, offering a refined focus on the interaction within the designated cavity. The results of docking studies on the mentioned targets are shown in Table I and Fig. S-3 (Supplementary material).

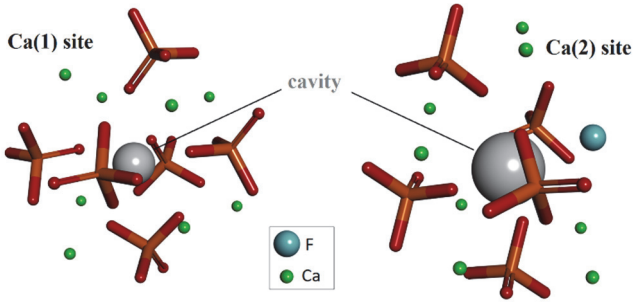

Fig. 4. The structures of targets, Ca(1) site and Ca(2) site, used for the docking study.

Results of docking studies with Ca^{2+}

The docking study showed that the Ca^{2+} has a slightly higher binding energy for Ca(2) site (ΔG_2 = –70.7 kJ mol^{-1}) than for Ca(1) site (ΔG_1 = –70.0 kJ mol^{-1}). The disparity in affinity towards specific sites is quantified by the $\Delta\Delta G_{1-2}$ para-

meter ($\Delta\Delta G_{1-2} = \Delta G_1 - \Delta G_2$), where a positive value denotes a heightened affinity for Ca(2) site. For the Ca^{2+}, the $\Delta\Delta G_{1-2}$ value is merely 0.7 kJ mol^{-1}, indicating a subtle predilection for binding to Ca(2) site. This outcome aligns with expectations derived from the analysis of parameters acquired through the CSD search. The distribution of Ca–O bond lengths (Fig. 2) reveals a peak in the range of 2.3 to 2.5 Å, supporting the notion of calcium ions favouring binding to Ca(2) site. The average Ca–O bond length in Ca(2) site (2.441 Å) is shorter than that in Ca(1) site (2.524 Å). The analysis of the number of atoms bound to calcium in crystal structures (Fig. 2) further reinforces the preference for binding to Ca(2) site. The structures with seven atoms bound to calcium (a geometric feature of Ca(2) site) are five times more prevalent than those with nine atoms bound to calcium (a geometric feature of Ca(1) site). DFT calculations indicate that the electrostatic interactions between the Ca^{2+} and the phosphate group at distances of 2.4 Å are stronger than interactions at approximately 2.6 Å (Fig. 3). This suggests that binding with shorter Ca–O distances, characteristic of Ca(2) site, is energetically favoured. Overall, the combination of docking studies, structural analysis, and DFT calculations provides comprehensive insights into the preferential binding behaviour of Ca^{2+} at distinct sites. The results of conventional molecular docking simulations are not consistent with the electrostatic model (Table I).

TABLE I. Gibbs energies changes (kJ mol^{-1}) for binding of investigated metal ions (ligands) to Ca(1) and Ca(2) sites, obtained by molecular docking with electrostatic model and conventional model

Ligand	ΔG_1	ΔG_2	$\Delta\Delta G_{1-2}$	$\Delta\Delta G_{11}$	$\Delta\Delta G_{22}$
Molecular docking with electrostatic model					
Ca^{2+}	–70.0	–70.7	+0.7	0	0
Sr^{2+}	–51.0	–54.5	+3.5	–19.0	–16.2
Mn^{2+}	–80.5	–78.9	–1.6	+9.5	+8.2
Cu^{2+}	–61.9	–68.8	+6.9	–8.1	–1.9
Pr^{3+}	–93.3	–100.4	+7.1	+23.3	+29.7
Conventional molecular docking model					
Ca^{2+}	–61.3	–53.1	–8.2	0	0
Sr^{2+}	–44.2	–14.1	–30.1	–17.1	–39.0
Mn^{2+}	–66.5	–59.0	–7.5	+5.2	+5.9
Cu^{2+}	–52.1	–44.9	–7.2	–9.2	–8.2
Pr^{3+}	–78.5	–66.5	–12.0	+17.2	+13.5

Results of docking studies with Sr^{2+}

To investigate the impact of an increase in ionic radius on the binding affinity, without altering the charge or nature of the ion, docking study was conducted with Sr^{2+}. Strontium is a metal of s-block elements, like calcium. Sr^{2+} is significantly larger (1.31 Å for nine-coordinated and 1.21 Å for seven-coordinated strontium) than Ca^{2+} (1.18 Å for nine-coordinated and 1.06 Å for seven-coordinated cal-

cium).[16] In this case, there is no agreement in the prediction of binding affinity between the analysis of crystal structures from CSD and the results of DFT calculations. The distribution of Sr–O bond lengths (Fig. 2) peaks in the range of 2.5 to 2.7 Å, suggesting higher affinity of Sr^{2+} for binding to Ca(1) site. A threefold higher occurrence of crystal structures with nine bound atoms to Sr (Fig. 2) supports this prediction. Conversely, DFT calculations indicate the most stable orientation of the phosphate group and Sr^{2+} at 2.4 Å, indicating a higher binding affinity for Sr^{2+} to Ca(2) site, characterized by shorter M–O bonds than Ca(1) site. Docking study results further confirm a slightly higher binding energy for Sr^{2+} at Ca(2) site (ΔG_2 = –54.5 kJ mol^{-1}) compared to Ca(1) site (ΔG_1 = –51.0 kJ mol^{-1}), with a $\Delta\Delta G_{1-2}$ of 3.5 kJ mol^{-1}, signifying a slight affinity for Ca(2) site. The disparity in Sr–O bond lengths in crystal structures (ranging from 1.9 to 3.0 Å) is attributed to structural diversity and varying charges of oxygen species bound to strontium. The prevalence of neutral oxygen species leads to longer Sr–O bonds, affecting the reliability of Sr–O bond length distribution in crystal structures for predicting binding affinity in the molecular docking system. The $\Delta\Delta G_{1-2}$ parameter alone is insufficient for prediction of structural changes of materials due to doping. The additional parameters, $\Delta\Delta G_{11}$ and $\Delta\Delta G_{22}$ (Table I), represent the differences between ΔG values for calcium and doped ions in each site. The positive values indicate fluorapatite structure stabilization due to doping. Sr^{2+} doping induces slight destabilization, more pronounced for Ca(1) site. Lower binding free energies for Sr^{2+} in both sites ($\Delta\Delta G_{11}$ and $\Delta\Delta G_{22}$) align with weaker interactions observed in DFT calculations, where Sr^{2+} form fewer coordination bonds than Ca^{2+}. Considering $\Delta\Delta G_{11}$, $\Delta\Delta G_{22}$ and $\Delta\Delta G_{1-2}$ parameters, Sr^{2+} exhibits a higher affinity for binding to Ca(2) site, but binding in both sites is possible. The results of the docking study have shown excellent agreement with the data obtained from the crystal structures of natural Sr-substituted fluorapatites, archived in the American Mineralogist Crystal Structure Database (AMCSD).[17] Namely, 38 fluorapa0-tite structures were found in the database, of which two structures have doped strontium ions.[6] In these structures, the Sr^{2+} prefers binding in Ca(2) site, although a small number of ions are doped in Ca(1) site as well. In the first structure (database code amcsd 0001421), the site-occupancy of Sr^{2+} is 0.016 for Ca(1) site and 0.094 for Ca(2) site, while in the second structure (database code amcsd 0001422), the site occupancy for Ca(1) site is 0.002 and for Ca(2) site is 0.048. The results of conventional molecular docking simulations are not consistent with the experimental results, indicating a higher affinity of Sr^{2+} to the Ca(1) site (Table I).

Results of docking studies with Mn^{2+}

In order to investigate the impact of reducing the ionic radius, while keeping the charge constant, on binding the affinity, a docking study was conducted using Mn^{2+}. Manganese, belonging to the d-block elements, is situated in period 4 of the

Periodic Table, analogous to calcium. Analysis of data retrieved from the Crystal Structure Database (CSD) reveals that Mn^{2+} forms notably shorter M–O bonds, with a peak in the range of 2.1 to 2.3 Å (Fig. 2), compared to calcium ion in both binding sites. Manganese exhibits a propensity to form compounds with six bonded atoms, adopting an octahedral geometry (Fig. 2). Nevertheless, there exists the possibility of forming complexes with seven bonded atoms, corresponding to the geometry observed in Ca(2) site. In addition, there are no structures with nine bonded atoms for manganese (corresponding to Ca(1) site-geometry). Results of DFT calculations (Fig. 3) have shown that Mn^{2+} forms significantly stronger interactions with the phosphate group (interaction energy of –3350 kJ mol^{-1}) than Ca^{2+} (interaction energy of –2500 kJ mol^{-1}). This analysis suggests that Mn^{2+} is likely to exhibit a greater binding free energy than calcium, although specific predictions regarding its affinity to a particular binding site remain indeterminate. The results from the docking study (Table I) reveal a slightly elevated binding free energy for the Mn^{2+} at Ca(1) site (ΔG_1 = –80.5 kJ mol^{-1}) compared to Ca(2) site (ΔG_2 = –78.9 kJ mol^{-1}). The $\Delta\Delta G_{1-2}$ value of –1.6 kJ mol^{-1} indicates a marginal preference for binding to Ca(1) site, with the possibility of binding to Ca(2) site. However, this site-specific affinity is less pronounced when compared to Sr^{2+} ($\Delta\Delta G_{1-2}$ value of +3.5 kJ mol^{-1}). Positive values of $\Delta\Delta G_{11}$ and $\Delta\Delta G_{22}$ parameters (9.5 and 8.2 kJ mol^{-1}, respectively) indicate stabilization of the fluorapatite structure due to doping of Mn^{2+}, which is slightly pronounced for site 1. Stabilization of fluorapatite structure upon doping with Mn^{2+} can be explained by stronger interactions with phosphate groups, compared to Ca^{2+} (Fig. 3). In Ca(1) site, the Mn^{2+} forms a tetrahedral complex (four bound atoms), with Mn–O bond lengths of 1.566, 1.908, 2.015 and 2.758 Å (mean value of 2.062 Å). In Ca(2) site, the Mn^{2+} forms a square-pyramidal complex (five bound atoms), with Mn–O bond lengths of 2.311, 2.507, 2.593 and 2.647 Å (mean value of 2.514 Å), as well as the Mn–F bond with length of 1.549 Å. Mn^{2+} is significantly smaller (0.66 Å for four--coordinated and 0.75 Å for five-coordinated manganese) than Ca^{2+} (1.18 Å for nine-coordinated and 1.06 Å for seven-coordinated calcium).[16] Even though Ca(2) site has more bound atoms, the significantly longer bond lengths likely account for the diminished binding strength of Mn^{2+} to this site. The outcomes of the docking study exhibit the remarkable congruence with data derived from crystal structures of naturally occurring Mn-substituted fluorapatites within the American Mineralogical Crystal Structure Database (AMCSD). Two distinct structures featuring doped manganese ions are identified.[6] In both structures, Mn^{2+} displays a preference for binding at Ca(1) site, with a minor presence at Ca(2) site. In the first structure (database code: 0001423), the site occupancy of Mn^{2+} is 0.205 for Ca(1) site and 0.065 for Ca(2) site. Similarly, in the second structure (database code: 0001424), the site-occupancy for Ca(1) site is 0.083, while that for Ca(2) site is 0.015. Although the results of conventional molecular docking simulations showed

that Mn^{2+} is bound stronger to both sites than Ca^{2+}, it is not consistent with the experimental results, because it refers to the tendency of Mn^{2+} to bound only to Ca(1) sites (Table I).

Results of docking studies with Cu^{2+}

Despite their comparable sizes, Cu^{2+} exhibits a distinct binding affinity compared to Mn^{2+}. Specifically, the Rietveld analysis of the hexagonal crystal structure of synthesized Cu^{2+}-doped fluorapatite indicates a preference for Cu^{2+} to selectively substitute for Ca^{2+} at Ca(2) site.[18] An examination of data obtained from the CSD reveals that Cu^{2+} establishes considerably shorter M–O bonds than calcium ions in both binding sites. The distribution of M–O bond lengths exhibits a conspicuous peak within the range of 1.9 to 2.0 Å, accompanied by a secondary, less pronounced peak spanning from 2.3 to 2.4 Å (Fig. 2). Analogous to manganese, copper compounds predominantly feature six atoms bound to copper, while those with five bonded atoms are notably prevalent (Fig. 3). There exists a potential for forming complexes with seven and nine bound atoms, corresponding to geometries at Ca(2) site and Ca(1) site, respectively (Fig. 2). Geometrical analysis of data from the CSD base suggests a resemblance in the binding patterns of Cu^{2+} with Mn^{2+} to fluorapatite. The results derived from the docking study (Table I) reveal that Cu^{2+} manifests a significantly lower binding free energy at Ca(1) site ($\Delta G_1 = -61.9$ kJ mol^{-1}) in comparison to Ca(2) site ($\Delta G_2 = -68.8$ kJ mol^{-1}). The positive value of $\Delta\Delta G_{1-2}$ parameter (6.9 kJ mol^{-1}) indicates affinity for binding to Ca(2) site; however, as this value is greater than 5 kJ mol^{-1}, it should be expected that Cu^{2+} is bound only to Ca(2) site. The findings from the docking study align with the outcomes of Rietveld analysis,[18] confirming the exclusive binding of Cu^{2+} to Ca(2) site. The negative values for $\Delta\Delta G_{11}$ and $\Delta\Delta G_{22}$ parameters (–8.1 and –1.9 kJ mol^{-1}, respectively) signify a destabilization effect on the fluorapatite structure resulting from the incorporation of Cu^{2+}. This destabilization phenomenon was observed in a crystal structure where the substitution of Ca^{2+} by Cu^{2+} occurred.[19] Although the interaction energy of Mn^{2+} with the phosphate group (of –3350 kJ mol^{-1}, Fig. 3) is lower than the energy of the interaction involving the Cu^{2+} (of –3770 kJ mol^{-1}, Fig. 3), the binding free energy change of the Mn^{2+} is still higher. This disparity can be attributed to the geometric characteristics of the resulting complexes at both binding sites. In Ca(1) site, Cu^{2+} forms a tetrahedral complex characterized by four bound atoms, with Cu–O bond lengths measuring 2.225, 2.389, 2.561 and 2.606 Å (mean value of 2.445 Å). The average length of the Cu–O bond is notably longer than that observed for Mn^{2+} (mean value of 2.062 Å), which likely contributes to the higher binding free energy of Mn^{2+} at Ca(1) site. At Ca(2) site, Cu^{2+} adopts a square-pyramidal configuration involving five bound atoms, with Cu–O bond lengths of 1.940, 2.336, 2.489 and 2.643 Å (mean value of 2.352 Å). However, a significantly elongated Cu–F bond (length of 2.716

Å) is observed in comparison to Mn^{2+} (Mn–F bond with a length of 1.549 Å). Based on the findings from the docking study, it can be inferred that the binding of Mn^{2+} and Cu^{2+} induces a reduction in the M–O bond length compared to undoped fluorapatite. Notably, in nanocrystals of Cu^{2+}-doped fluorapatite, M–O distances were observed to be shorter with an increasing concentration of doped Cu^{2+}.[19] The ionic radius of the Cu^{2+} in both binding sites (0.57 Å for four-coordinated and 0.65 Å for five-coordinated manganese) is marginally smaller than that of Mn^{2+} and significantly diminutive compared to the radius of the Ca^{2+}.[16] Consequently, the substitution of Ca^{2+} by Cu^{2+} in Ca(2) site induces a reduction in the stability of the fluorapatite structure, leading to structural distortions. These alterations are discernible through a decrease in the height of the apatite peaks[19] and an enhanced thermal stability observed in the fluorapatite sample in contrast to Cu^{2+}-doped fluorapatite.[18] The destabilization of the fluorapatite structure, as evidenced by DTA–TGA studies, has also been observed in structures doped with Ag, Cd and Zn ions.[20–22] The results of conventional molecular docking are not consistent with the experimental results, because it refers to the tendency of Cu^{2+} to bound only to Ca(1) sites (Table I).

Results of docking studies with Pr^{3+}

Pr^{3+} was chosen to determine the effect of increasing charge on binding affinity to a specific site in fluorapatite. In light of the distribution of Pr–O bond lengths, characterized by a peak within the range of 2.4 to 2.6 Å (Fig. 2), a preference for the binding of Pr^{3+} to any specific site cannot be established. This is due to the fact that the mean values of Ca–O bond lengths in Ca(1) site and Ca(2) site falls within this range, measuring 2.524 and 2.441 Å, respectively. Pr^{3+} forms slightly longer M–O bonds, compared to Ca^{2+}, whose distribution of M–O bonds has a maximum in the range from 2.3 to 2.5 Å (Fig. 2). Within crystal structures, praseodymium compounds featuring eight bonded atoms are predominant, as illustrated in Fig. 2. Notably, the incidence of structures with seven atoms bound to praseodymium, corresponding to the coordination geometry observed at Ca(2) site, significantly surpasses the occurrence of structures with nine atoms bound to praseodymium, corresponding to the coordination geometry observed at Ca(1) site. Based on this parameter, it can be assumed that Pr^{3+} has a higher binding affinity to Ca(2) site. The results of molecular docking have confirmed this assumption. Namely, the Pr^{3+} has a significantly smaller binding free energy to Ca(1) site (ΔG_1 = –93.3 kJ mol^{-1}) than to Ca(2) site (ΔG_2 = –100.4 kJ mol^{-1}). Positive value of $\Delta\Delta G_{1-2}$ parameter (7.1 kJ mol^{-1}) indicates the affinity for binding to Ca(2) site; however, as its value is greater than 5 kJ mol^{-1}, it should be expected that Pr^{3+} is bound only to Ca(2) site. The positive values recorded for the $\Delta\Delta G_{11}$ and $\Delta\Delta G_{22}$ parameters (23.3 and 29.7 kJ mol^{-1}, respectively) signify the stabilization of the fluorapatite structure resulting from the incorporation of Pr^{3+}. The prior assessments of site-

-occupancy ratios for rare earth elements in natural fluorapatites have been conducted, and the determined ratio for Pr^{3+} underscores a predominant preference for the Ca(2) site.[9,23] Observationally, the binding free energy changes of Pr^{3+}, as documented in Table I, exhibit a notable increase compared to those of Ca^{2+}. This marked difference can likely be attributed to the more robust interactions of the Pr^{3+} with the phosphate group, denoted by an interaction energy of –5000 kJ mol^{-1} (Fig. 3), in contrast to the interactions of this group with Ca^{2+}, characterized by an interaction energy of –2500 kJ mol^{-1}. The possible reason can be also found in the geometry of the resulting complexes in both sites. In Ca(1) site, Pr^{3+} forms a seven-coordinated polyhedron, with Pr–O bond lengths of 2.225, 2.251, 2.477, 2.511, 2.561, 2.606 and 2.772 Å (mean value of 2.486 Å). The mean Pr–O bond length is comparatively shorter than the mean Ca–O bond length observed at Ca(1) site, with a recorded mean value of 2.524 Å. Pr^{3+} adopts a six-coordinated polyhedron at Ca(2) site, forming Pr–O bond lengths of 1.940, 2.163, 2.336 and 2.843 Å, resulting in a mean bond length of 2.354 Å. Additionally, a Pr–F bond with a length of 2.716 Å is present. Notably, at Ca(2) site, the mean value of the Pr–O bond length is smaller than the corresponding value observed for Ca^{2+}, which is recorded at a mean value of 2.441 Å. The outcomes of DFT calculations reveal that the energetic strength of interactions between Pr^{3+} and the phosphate group is greater at a distance of 2.3 Å, compared to interactions at a distance of 2.4 Å. This observation potentially elucidates the elevated binding free energy change of Pr^{3+} at Ca(2) site. The reduced mean M–O bond lengths for Pr^{3+}, as compared to corresponding values for Ca^{2+}, arise from the higher positive charge of the praseodymium ion, leading to intensified electrostatic interactions between metal ions and negatively charged species (phosphate groups and fluoride ions) within both sites. This phenomenon may provide a plausible explanation for alterations in lattice parameters and reductions in crystallite size observed in Pr^{3+}-doped fluorapatite samples relative to pure fluorapatite.[24] Although the results of conventional molecular docking simulations showed that Pr^{3+} is bound stronger to both sites than Ca^{2+}, it is not consistent with the experimental results, because it refers to the tendency of Pr^{3+} to bound only to Ca(1) sites (Table I).

CONCLUSION

The presented findings unequivocally demonstrate the successful attainment of the primary research objective. Notably, this study establishes, for the first time, the efficacy of molecular docking with electrostatic model in making material-related predictions, extending its utility beyond the conventional realm of assessing small molecule (ligand) binding to biomolecules (targets). Although the conventional molecular docking simulations are commonly used for predicting the binding of small molecules to materials, such as metal–organic frameworks (MOFs),[25–27] in our case, they proved to be ineffective. However, the application

of the molecular docking with an electrostatic model yielded results that exhibited excellent agreement with experimental data. This not only lends an innovative character to our approach but also demonstrates its scientific potential in predicting binding to materials representing ionic compounds, such as fluorapatite. The investigation focused on evaluating the binding strength of fluorapatite with five metal ions (Ca^{2+}, Sr^{2+}, Mn^{2+}, Cu^{2+} and Pr^{3+}) for the purpose of predicting site-preference and discerning alterations in the stability of crystal structures resulting from fluorapatite doping with these ions. The selected metal ions exhibit varying ionic radii – smaller in the case of Mn^{2+} and Cu^{2+}, larger for Sr^{2+}, and comparable but with a higher charge for Pr^{3+}, when contrasted with Ca^{2+}. These differences in ionic radii and charges significantly influence the site-preference of metal ion binding, as determined through site-occupancy, and contribute to changes in the stability of doped fluorapatite crystal structures, as indicated by alterations in the height of the apatite X-ray diffraction (XRD) peaks. The molecular docking was here employed to predict site-preferences and quantitatively characterize the stability of structures, demonstrating a surprising concordance with experimentally measured values in doped fluorapatites. This remarkable agreement strongly supports the applicability of molecular docking in materials research. Utilizing molecular docking in the biomaterials domain can facilitate the discovery of novel structures with multifunctional attributes for biomedical uses. Moving forward, the team plans to expand the repertoire of metal ions for theoretical binding predictions to fluorapatite and explore the applicability of molecular docking in other material systems.

SUPPLEMENTARY MATERIAL

Additional data and information are available electronically at the pages of journal website: https://www.shd-pub.org.rs/index.php/JSCS/article/view/13235, or from the corresponding author on request.

Acknowledgement. This work was supported by the Ministry of Science, Technological Development and Innovation of the Republic of Serbia (Contracts No. 451-03-66/2024-03/ /200162, 451-03-66/2024-03/200023 and 451-03-66/2024-03/200026).

ИЗВОД

ПИОНИРСКА УЛОГА МОЛЕКУЛСКОГ ДОКИНГА У НАУЦИ О МАТЕРИЈАЛИМА. ПРЕФЕРЕНТНА ВЕЗИВНА МЕСТА ЈОНА МЕТАЛА У ФЛУОРАПАТИТУ

МАРИЈА М. ПЕТКОВИЋ-БЕНАЗУЗ[1], ИГОР РАДОВИЋ[2], ДУШАН В. МИЛОЈКОВ[3] и ГОРАН ЈАЊИЋ[4]

[1]Универзитет у Београду–Физички факултет, Студентски трг 12, Београд, [2]Катедра за дентални патологију, Медицински факултет, Универзитет у Источном Сарајеву, Студентска 5, Фоча, Босна и Херцеговина, [3]Институт за технологију нуклеарних и других минералних сировина, Франше д'Епереа 86, Београд и [4]Универзитет у Београду–Институт за хемију, технологију и металургију, Институт од националног значаја за Републику Србију, Његошева 12, Београд

Првобитно намењен за биолошке системе, молекулски докинг се се показао као вишенаменски, јер се може користити и за предвиђање места везивања јона метала и

њихових афинитета у материјалима. Коришћењем овог новог приступа, могуће је проценити енергије везивања Ca^{2+}, Sr^{2+}, Mn^{2+}, Cu^{2+} и Pr^{3+} за два различита места везивања јона метала у флуорапатиту. Подаци добијени из кристалних структура допираних флуорапатита показали су добру сагласност са докинг студијом. Интерпретација резултата молекулског докинга је употуњена комбиновањем са резултатима DFT прорачуна, и са геометријском анализом кристалних структура малих молекула. Очигледно је да је ова нова стратегија погоднија од других теоријских приступа, због своје рачунарске сврсисходности, брзине и поузданости.

(Примљено 2. фебруара, ревидирано 11. марта, прихваћено 11. априла 2025)

REFERENCES

1. K. Pajor, L. Pajchel, J. Kolmas, *Materials* **12** (2019) 2683 (https://doi.org/10.3390/ma12172683)
2. N. Leroy, E. Bres, *Eur. Cell Mater.* **30** (2001) 36 (https://doi.org/10.22203/eCM.v002a05)
3. J. C. Elliott, *Structure and chemistry of the apatites and other calcium orthophosphates. Studies in inorganic chemistry*, Elsevier, Amsterdam, 1994 (ISBN: 9780444815828)
4. E. R. Kreidler, F. A. Hummel, *Am. Min.* **55 (**1970) 170.
5. D. V. Milojkov, V. Đ. Stanić, S. D. Dimović, D. R. Mutavdžić, V. Živković-Radovanović, G. V. Janjić, K. Radotić, *Acta Phys. Pol., A* **136** (2019) 86 (https://dx.doi.org/10.12693/APhysPolA.136.86)
6. J. M. Hughes, M. Cameron, K. D. Crowley, *Am. Min.* **76** (1991) 1857 (http://www.minsocam.org/ammin/AM76/AM76_1857.pdf)
7. M. Miyake, K. Ishigaki, T. Suzuki, *J. Solid State Chem.* **61** (1986) 230 (https://doi.org/10.1016/0022-4596(86)90026-5)
8. D. V. Milojkov, M. D. Sokić, V. Živković-Radovanović, V. D. Manojlović, D. R. Mutavdžić, G. V. Janjić, K. Radotić, *Opt. Quantum Electron.* **55** (2023) 84 (https://dx.doi.org/10.1007/s11082-022-04347-7)
9. M. E. Fleet, Y. Pan, *Am. Min.* **82** (1997) 870 (https://doi.org/10.2138/am-1997-9-1004)
10. P. E. Mackie, R. A. Young, *J. Appl. Crystallogr.* **6** (1973) 26 (https://doi.org/10.1107/S0021889873008009)
11. X. Li, J. Zhu, Z. Man, Y. Ao, H. Chen, *Sci. Rep.* **4446** (2014) 4446 (https://dx.doi.org/10.1038/srep04446)
12. C. R. Groom, I. J. Bruno, M. P. Lightfoot, S.C. Ward, *Acta Crystallogr., B* **72** (2016) 171 (https://doi.org/10.1107/S2052520616003954)
13. J. M. Hughes, M. Cameron, K. D. Crowley, *Am. Min.***74** (1989) 870
14. G. M. Morris, R. Huey, W. Lindstrom, M.F. Sanner, R.K. Belew, D.S. Goodsell, A.J. Olson, *J. Comput. Chem.* **16** (2009) 2785 (https://doi.org/10.1002/jcc.21256)
15. D. Biovia, H. Berman, J. Westbrook, Z. Feng, G. Gilliland, T. Bhat, T.J.T.J.o.C.P. Richmond, Dassault Systèmes BIOVIA, Discovery Studio Visualizer, v. 17.2.0.16349, Dassault Systèmes, San Diego, CA, 2016, 10 (2000) 0021-9991
16. R. D. Shannon, *Acta Crystallogr., A* **32** (1976) 751 https://doi.org/10.1107/S0567739476001551)
17. R. T. Downs, M. Hall-Wallace. *Am. Min.* **88** (2003) 247
18. D. V Milojkov, A. S Radosavljević-Mihajlović, V. Đ. Stanić, B. J Nastasijević, K. Radotić, I. Janković-Častvan, V. Živković-Radovanović, *J. Photochem. Photobiol. B: Biology* **239** (2023) 112649 (https://doi.org10.1016/j.jphotobiol.2023.112649)

19. R. Nikonam Mofrad, S. K. Sadrnezhaad, J. Vahdati Khaki, *Sci. Iranica, B* **24** (2017) 2845 (https://doi.org/10.24200/sci.2017.4314)
20. V. Đ. Stanić, A. S. Radosavljević-Mihajlović, V. Živković-Radovanović, B. Nastasijević, M. Marinović-Cincović, J. P. Marković, M. D. Budimir, *Appl. Surf. Sci*. **337** (2015) 72 (https://doi.org/10.1016/j.apsusc.2015.02.065)
21. K. Tõnsuaadu, K. A. Gross, L. Plūduma, M. Veiderma, *J. Therm. Anal. Calorim*. **110** (2012) 647 (https://doi.org/10.1007/s10973-011-1877-y)
22. G. W. C. Silva, O. Hemmers, K. R. Czerwinski, D. W. Lindle, *Inorg. Chem*. **47** (2008) 7757 (https://doi.org/10.1021/ic800794x)
23. M. E. Fleet, Y. Pan, *Am. Min.* **80** (1995) 329 (https://doi.org/10.2138/am-1995-3-414)
24. D. V. Milojkov, O. F. Silvestre, V. Đ. Stanić, G. V. Janjić, D. R. Mutavdžić, M. Milanović, J. B. Nieder, *J. Lumi.* **217** (2020) 116757 (https://doi.org/10.1016/j.jlumin.2019.116757)
25. F. Keshavarz, B. Barbiellini, *Comput. Mater. Sci.* **226** (2023) 112257 (https://doi.org/10.1016/j.commatsci.2023.112257)
26. C. A. Anyama, H. Louis, B.E. Inah, T. E. Gber, J. O. Ogar, A. A. Ayi, *J. Mol. Struct.* **1277** (2023) 134825 (https://doi.org/10.1016/j.molstruc.2022.134825)
27. Q. Li, W. Zhang, O. Š. Miljanić, C.-H. Sue, Y.-L. Zhao, L. Liu, C. B. Knobler, J. F. Stoddart, O.M. Yaghi, Science **325** (2009) 855 (https://doi.org/10.1126/science.1175441).